Mineralogical Magazine, December 2016, Vol. 80(7), pp. 1243–1254

Kummerite, $Mn^{2+}Fe^{3+}Al(PO_4)_2(OH)_2{\cdot}8H_2O$, a new laueite-group mineral from the Hagendorf Süd pegmatite, Bavaria, with ordering of Al and Fe^{3+}

I. E. Grey[1,*], E. Keck[2], W. G. Mumme[1], A. Pring[3], C. M. Macrae[1], A. M. Glenn[1], C. J. Davidson[1], F. L. Shanks[4] and S. J. Mills[5]

[1] CSIRO Mineral Resources, Private Bag 10, Clayton South, Victoria 3169, Australia
[2] Algunderweg 3, D-92694 Etzenricht, Germany
[3] Department of Mineralogy, South Australian Museum, North Terrace, Adelaide, South Australia 5000, Australia
[4] School of Chemistry, Monash University, Clayton, Victoria 3800, Australia
[5] Geosciences, Museum Victoria, GPO Box 666, Melbourne, Victoria 3001, Australia

[*Received 31 August 2015; Accepted 16 November 2016; Associate Editor: Stuart Mills*]

ABSTRACT

Kummerite, ideally $Mn^{2+}Fe^{3+}Al(PO_4)_2(OH)_2{\cdot}8H_2O$, is a new secondary phosphate mineral belonging to the laueite group, from the Hagendorf-Süd pegmatite, Hagendorf, Oberpfalz, Bavaria, Germany. Kummerite occurs as sprays or rounded aggregates of very thin, typically deformed, amber yellow laths. Cleavage is good parallel to {010}. The mineral is associated closely with green Zn- and Al-bearing beraunite needles. Other associated minerals are jahnsite-(CaMnMn) and Al-bearing frondelite. The calculated density of kummerite is 2.34 g cm^{-3}. It is optically biaxial (–), $\alpha = 1.565(5)$, $\beta = 1.600(5)$ and $\gamma = 1.630(5)$, with weak dispersion. Pleochroism is weak, with amber yellow tones. Electron microprobe analyses (average of 13 grains) with H_2O and FeO/Fe_2O_3 calculated on structural grounds and normalized to 100%, gave Fe_2O_3 17.2, FeO 4.8, MnO 5.4, MgO 2.2, ZnO 0.5, Al_2O_3 9.8, P_2O_5 27.6, H_2O 32.5, total 100 wt.%. The empirical formula, based on 3 metal apfu is $(Mn^{2+}_{0.37}Mg_{0.27}Zn_{0.03}Fe^{2+}_{0.33})_{\Sigma 1.00}(Fe^{3+}_{1.06}Al_{0.94})_{\Sigma 2.00}PO_4)_{1.91}(OH)_{2.27}(H_2O)_{7.73}$. Kummerite is triclinic, $P\bar{1}$, with the unit-cell parameters of $a = 5.316(1)$ Å, $b = 10.620(3)$ Å , $c = 7.118(1)$ Å, $\alpha = 107.33(3)°$, $\beta = 111.22(3)°$, $\gamma = 72.22(2)°$ and $V = 348.4(2)$ $Å^3$. The strongest lines in the powder X-ray diffraction pattern are [d_{obs} in Å(I) (*hkl*)] 9.885 (100) (010); 6.476 (20) (001); 4.942 (30) (020); 3.988 (9) ($\bar{1}10$); 3.116 (18) ($1\bar{2}0$); 2.873 (11) ($\bar{1}21$). Kummerite is isostructural with laueite, but differs in having Al and Fe^{3+} ordered into alternate octahedral sites in the 7.1 Å *trans*-connected octahedral chains.

Keywords: kummerite, new laveite-group mineral, Al-Fe ordering, synchrotron single-crystal study.

Introduction

Nature provides intriguing examples of minerals with the same generic composition and with topologically similar heteropolyhedral structures, but with subtle changes in the orientation and connectivity of the polyhedra that reflect different conditions under which the minerals were formed.

In graph terminology applied to crystallography (Hawthorne, 1983) the minerals have the same topology of connections between polyhedra (same topological isomers) but they differ in the relative orientation of the polyhedra or in having different relative locations of the anions (*cis*- or *trans*-) involved in the connections (different geometric isomers). Examples include uranyl phosphate minerals of the phosphuranylite group (Locock and Burns, 2003), and minerals with sheet structures built from kröhnkite-type chains (Fleck *et al*., 2002), both of which involve orientation

*E-mail: Ian.Grey@csiro.au
DOI: 10.1180/minmag.2016.080.061

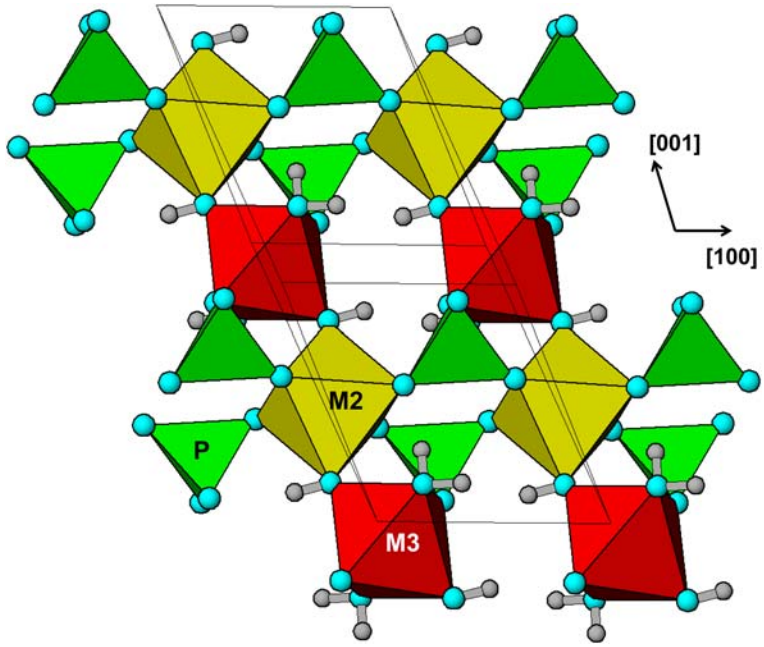

FIG. 1. The heteropolyhedral (010) sheet in laueite. Small grey and blue spheres are hydrogen and oxygen.

isomerism of tetrahedra. Examples of *cis-trans* isomerism occurs in the sheet structures of olmsteadite and rhomboclase (Hawthorne, 1985) and in chain structures involving kröhnkite-type chains (Krivovichev, 2004).

Particularly diverse isomerism occurs in minerals with structures containing laueite-type sheets, $M_2(XO_4)_2\Phi_4$, of corner-connected octahedra and tetrahedra. These include the laueite, pseudolaueite, stewartite and metavauxite structure types, described as combinatorial polymorphs by Moore (1975). Krivovichev (2004) has analysed these minerals and synthetic equivalents using graph theory and separated them into different classes of topological and geometric isomers. Laueite and stewartite share the same topology but are different geometrical isomers based on orientations of the tetrahedra, while pseudolaueite and metavauxite are geometric isomers corresponding to a different topology. In the former minerals half the octahedra are connected to four tetrahedra while half are connected to two tetrahedra, whereas in the latter the different topology results from all octahedra having corner-connections to three tetrahedra.

The laueite-group minerals have the structural formula $M1^{2+}(H_2O)_4[M2^{3+}M3^{3+}(XO_4)_2(OH)_2(H_2O)_2]\cdot 2H_2O$, where the interlayer octahedral site $M1 = Fe^{2+}$, Mg^{2+} or Mn^{2+}; $M2/M3 = Al^{3+}$ or Fe^{3+}; and $XO_4 = PO_4$ or AsO_4. The heteropolyhedral sheet in laueite-group minerals with atom labelling is shown in Fig. 1. The laueite structure type is the most abundant of the four different structure types and Krivovichev (2004) suggested it is because it has the simplest 2D graph. Since the study by Krivovichev (2004) a number of new phosphate and arsenate minerals having the laueite structure have been described (Segeler *et al*., 2012; Meisser *et al*., 2012; Scholz *et al*., 2014) leading to the establishment of a nomenclature scheme for the laueite-supergroup minerals (Mills and Grey, 2015). The supergroup is divided into the laueite group (phosphates) and maghrebite group (arsenates) then further divided into subgroups on the basis of the dominant trivalent cations, Al^{3+} or Fe^{3+}, in octahedral sites *M*2/*M*3.

All reported laueite-supergroup minerals have either dominant Fe or dominant Al in both the *M*2 and *M*3 sites. Laueite itself, $Mn^{2+}Fe_2^{3+}(PO_4)_2(OH)_2\cdot 8H_2O$ (Strunz, 1954), has Fe^{3+} in both octahedral sites. The two sites have different coordinations and formal charges $[M2O_4(OH)_2]^{7-}$ and $[M3O_2(OH)_2(H_2O)_2]^{3-}$, respectively, for trivalent *M* cations and so ordering might be expected of different cations in the two sites. Such ordering in fact occurs in a number of synthetic phases having the laueite structure type. These include (enH_2)

https://doi.org/10.1180/minmag.2016.080.061 Published online by Cambridge University Press

$Fe_2F_2(HPO_4)_2(H_2O)_2$ (Cavellec *et al*., 1994), in which Fe^{3+} is ordered in *M*2 and Fe^{2+} in *M*3 and $(enH_2)NbFeOF(PO_4)_2(H_2O)_2$ (Wang *et al*. 2000), in which Nb^{5+} occupies *M*2 and Fe^{3+} occupies *M*3. In $(enH_2)Ti(Fe,Cr)(F,O)(H_{0.3}PO_4)_2(H_2O)_2$ (Wang *et al*. 2000), Ti^{4+} occupies *M*2 and Fe^{3+}/Cr^{3+} occupies *M*3.

In an on-going study on secondary phosphate minerals from the Hagendorf-Süd granitic pegmatite (Birch *et al*., 2011; Grey *et al*., 2010, 2012) we have recently reported on the preferential ordering of Al in the *M*3 site in laueite crystals that have undergone mineral replacement reactions (Grey *et al*., 2015). Crystal structure refinements for two crystals, L1 and L2, showed that the crystal L2, with the higher Al content, had dominant Al in the *M*3 site and dominant Fe^{3+} in the *M*2 site, thus qualifying it as a potential new mineral species. The IMA Commission on new Minerals, Nomenclature and Classification (IMA2015-036) approved the mineral and the name kummerite. The mineral is named for Rudolf Kummer (1924-1982), mining director of the Cornelia mine at Hagendorf Süd from 1964 until his death in 1982. Rudi had a great appreciation of, and familiarity with the mineral occurrences at the mine and he was very supportive of geologists, mineralogists and collectors who came to study and collect samples from the mine. The type specimen of kummerite is housed in the mineralogical collections of Museum Victoria, Melbourne, Victoria, Australia, registration number M53448.

Occurrence, mineral assemblage and paragenesis

Kummerite was found in specimens collected by one of the authors (EK) in the late 1970s at the 57 ± 2 m level of the Cornelia Mine Open Cut of the Hagendorf-Süd pegmatite, Hagendorf, Oberpfalz, Bavaria, Germany (49°39'1″N, 12°27'35″E). It is a very rare mineral that has been located in only a few specimens. Since 1984 the mine has been flooded and no further specimens can be collected.

Kummerite occurs in small cavities on altered zwieselite. It is closely associated with Zn- and Al-bearing beraunite, Al-bearing frondelite and jahnsite. Electron microprobe (EMP) analyses of the jahnsite gave a composition $Ca_{1.0}Mn_{2.2}Fe_{2.5}Mg_{0.2}Al_{0.1}(PO_4)_4(OH)_2{\cdot}8H_2O$, confirming it as jahnsite-(CaMnMn). This species of jahnsite has previously been found in association with nordgauite at Hagendorf-Süd and characterized using EMP analyses (Grey *et al.*, 2010).

Kummerite is a secondary phosphate mineral that has probably been formed from laueite by hydrothermal reaction with aluminium-bearing fluids. Support for such a paragenesis is that scanning electron microscope studies show that aggregates of kummerite laths generally surround a core of laueite composition.

Physical and optical properties

Kummerite forms sprays or rounded aggregates of very thin, typically deformed, amber yellow laths, associated intimately with green beraunite needles as shown in Fig. 2. The aggregates are commonly 100 to 500 μm in their longest dimension, but the individual lamellae, parallel to {010} have a thickness of the order of a few μm as shown in Fig. 3. The morphology and colour of kummerite is so similar to those for other laueite-related polymorphs and jahnsite that X-ray studies are essential for correct identification (Moore and Araki, 1974). Scanning electron microscope images of kummerite grains commonly display compositional zoning due to Al/Fe variations, as seen in Fig. 2 of Grey *et al.* (2015). The cores of the grains have compositions close to that for laueite and the rims are enriched in Al.

Kummerite crystals are brittle, have a vitreous lustre and are translucent. The streak is white. Cleavage is good parallel to {010}. The fracture is uneven. The crystals undergo severe fracturing and outgassing (dehydration) when placed in a high vacuum and the yellow colour becomes bleached, leaving silvery white crystals. The cracking of the

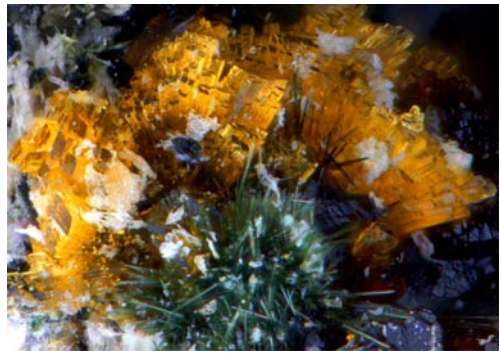

FIG. 2. Optical microscope picture of yellow kummerite laths and green beraunite needles. Field of view ≈ 2 mm.

https://doi.org/10.1180/minmag.2016.080.061 Published online by Cambridge University Press

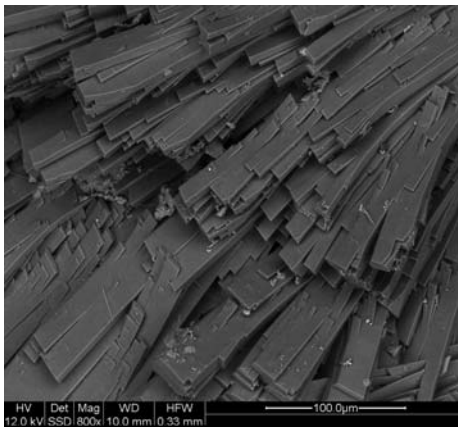

FIG. 3. Back-scattered electron image of kummerite laths.

crystals into small grains under high vacuum is illustrated in Fig. 4. The density could not be measured due to the very small grain size and intimate association with beraunite. The calculated density based on the empirical formula is 2.34 g cm^{-3}.

The optical characterization of kummerite was hampered by very fine-scale undulose extinction. The mineral is biaxial (–) with measured refractive indices $\alpha = 1.565(5)$, $\beta = 1.600(5)$ and $\gamma = 1.630(5)$ (white light). 2V could not be measured; $2V_{calc} = 84^{o}$. The crystals show weak dispersion. The orientation is uncertain. Pleochroism is weak, with amber yellow tones. The Gladstone-Dale compatibility index (Mandarino, 1981) calculated using the empirical formula and the calculated density is 0.016, which is classed as superior.

Other properties

Infrared spectroscopy

Attenuated total reflection infrared spectroscopy on individual crystals of kummerite was conducted using a Bruker IFS55 fitted with MCT detector and Specac diamond ATR. A total of 100 co-added scans were employed at a spectral resolution of 4 cm^{-1}. The infrared spectrum is shown in Fig. 5. The dominant feature in the spectrum is a strong broad envelope in the OH-stretching region, which has peaks at 3235 and 3530 cm^{-1} and shoulders at 2655, 2800 and 3375 cm^{-1}. The wide range of O–H vibrations is consistent with extensive H-bonds that range from weak to strong (Libowitzky, 1999). The H–O–H bending vibration for water molecules is at 1640 cm^{-1}. Only a single strong $(PO_4)^{3-}$ stretching vibration is resolved, at 985 cm^{-1}.

Chemical composition

Electron microprobe (EMP) analyses on Al-rich crystals were conducted using wavelength-dispersive spectrometry on a JEOL JXA 8500F Hyperprobe operated at an accelerating voltage of 12 kV and a beam current of 4 nA. The beam was defocused to 10 µm where the grain size permitted, otherwise it was 5 µm. The data were corrected for matrix effects using the ΦρZ method implemented in the JEOL system. Water could not be analysed directly because of the minute amount of sample available. Water was calculated on the basis of $8H_2O$ and $2OH^-$ per formula unit (pfu), consistent with the composition of laueite-group minerals.

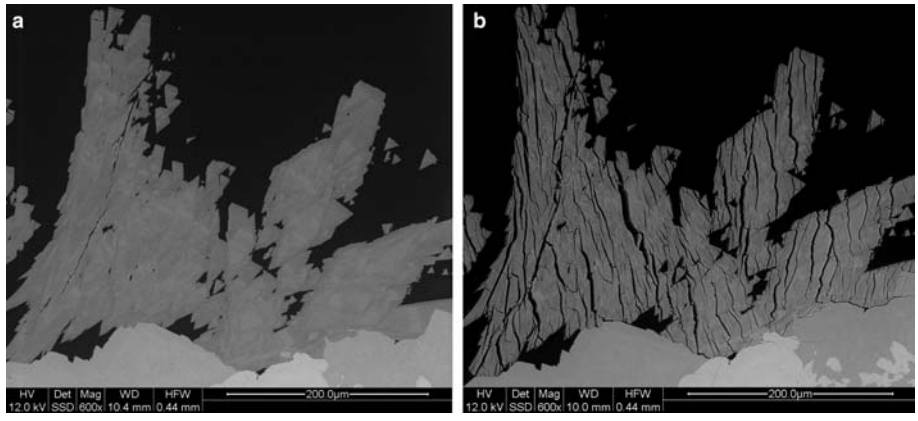

FIG. 4. Scanning electron microscope image of kummerite crystals: (*a*) in low vacuum (0.5 torr) and (*b*) after evacuation to 5×10^{-5} torr in the carbon coater.

https://doi.org/10.1180/minmag.2016.080.061 Published online by Cambridge University Press

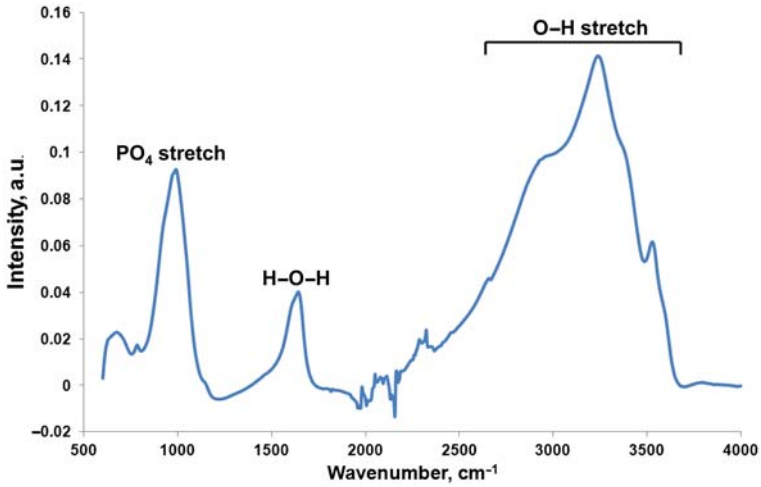

FIG. 5. Infrared spectrum for kummerite.

The results of analyses of 13 separate grains (13 analyses) are given in Table 1.

The high analysis total is due to dehydration and crystal cracking under vacuum as illustrated in Fig. 4. The cracking of the crystals into small grains restricted the amount of beam defocus that could be used to minimize further dehydration in the beam. This is common for highly hydrated minerals such as laueite. Analysis totals of 114 to 122% have been reported in three separate studies on laueite-related minerals, even though care was taken to defocus the beam to up to 25 μm or to scan the beam during the EMP analyses (Adiwidjaja *et al.*, 1999; Galliski and Hawthorne, 2002; Meisser *et al.*, 2012). Scaling the oxide analyses for kummerite in Table 1 so that the sum of oxides plus calculated water = 100% gives Fe_2O_3 17.2, FeO 4.8, MnO 5.4, MgO 2.2, ZnO 0.5, Al_2O_3 9.8, P_2O_5 27.6, H_2O, 32.5, sum 100.0 wt.%.

The empirical formula, based on 3 metal atoms pfu, with OH^- adjusted for charge balance is: $(Mn^{2+}_{0.37}Mg_{0.27}Zn_{0.03}Fe^{2+}_{0.33})_{\Sigma 1.00}(Fe^{3+}_{1.06}Al_{0.94})_{\Sigma 2.00}PO_4)_{1.91}(OH)_{2.27}(H_2O)_{7.73}$

The normalization was based on the metal atom sites rather than P because the structure analysis revealed a small deficiency in the P sites.

The simplified formula, with the dominant atom occupying each metal atom site and full occupancy of the P site is: $MnFe^{3+}Al(PO_4)_2(OH)_2 \cdot 8H_2O$.

TABLE 1. Analytical data (wt.%) for kummerite.

Constituent	Mean	Range	SD	Probe Standard
Fe_2O_3*	19.1			Hematite, Fe *K*α
FeO*	5.3			
MnO	5.9	4.4–8.5	1.5	$MnSiO_3$, Mn *K*α
MgO	2.4	1.5–3.5	0.5	$MgAl_2O_4$, Mg *K*α
ZnO	0.5	0–0.9	0.2	Phosphophyllite, Zn *L*α
Al_2O_3	10.7	8.2–14.4	2.1	$AlPO_4$, Al *K*α
P_2O_5	30.2	25.5–33.6	2.4	$AlPO_4$, P *K*α
H_2O**	32.5			
Total	106.6			

*Calculated from total Fe as Fe_2O_3 of 25.1 wt.%, range 21.7–30.5, SD (standard deviation) 2.5 on structure basis (Fe^{2+} in *M*1, Fe^{3+} in *M*2 and *M*3).
**H_2O calculated on the basis of $2OH^- + 8H_2O$ as in laueite-group minerals.

https://doi.org/10.1180/minmag.2016.080.061 Published online by Cambridge University Press

Crystallography

Powder X-ray diffraction

Powder X-ray diffraction data were collected at room temperature using a Philips XPert diffractometer with graphite-monochromatized Co$K\alpha$ radiation. The small quantity of crystals that were available was dispersed on a zero-background silicon disk for the data collection, the results of which are reported in Table 2. Indexation and refinement of 23 powder diffraction peak positions using *CELLREF* (Laugier and Bochu, 2000) gave the following cell parameters (triclinic, $P\bar{1}$): $a = 5.323(1)$, $b = 10.660(1)$, $c = 7.141(1)$ Å, $\alpha = 107.82(1)$, $\beta = 111.65(2)$, $\gamma = 71.76(1)°$ and $V = 349.3(9)$ Å^3.

Single-crystal studies

We have previously reported crystal structure refinements for two Al-bearing laueite crystals (Grey *et al.*, 2015). The higher-Al containing crystal, L2, gave refined site occupancies for the trivalent *M*2 and *M*3 sites of 0.67(1)Fe + 0.33Al and 0.48(1)Fe + 0.52Al respectively. The results for crystal L2 were used as the basis for a successful IMA naming proposal for kummerite, although the dominance of Al in site *M*3 is marginal. We have subsequently collected synchrotron single-crystal diffraction data on a new crystal, L3, for which the refinement gave a much more definitive ordering of dominant Fe in site *M*2 and dominant Al in site *M*3, the results of which are reported here.

TABLE 2. Powder diffraction data for kummerite.

I_{rel}	d_{meas} (Å)	d_{calc} (Å)	*h k l*
100	**9.885**	**9.886**	**0 1 0**
20	**6.476**	**6.481**	**0 0 1**
1	6.049	6.052	0 $\bar{1}$ 1
30	**4.942**	**4.943**	**0 2 0**
5	4.821	4.819	1 0 0
9	**3.988**	**3.991**	**$\bar{1}$ 1 0**
4	3.923	3.922	1 2 0
8	3.255	3.251	$\bar{1}$ $\bar{2}$ 2
9	**3.235**	**3.240**	**0 0 2**
18	**3.116**	**3.116**	**1 $\bar{2}$ 0**
2	3.062	3.062	1 3 0
11	**2.873**	**2.876**	**$\bar{1}$ 2 1**
2	2.713	2.711	0 3 1
6	2.615	2.614	$\bar{1}$ $\bar{4}$ 1
4	2.494	2.496	0 $\bar{4}$ 1
4	2.378	2.377	1 0 2
5	2.022	2.021	1 $\bar{4}$ 0
5	1.996	1.996	$\bar{2}$ 2 0
1	1.960	1.961	2 4 0
2	1.806	1.806	$\bar{1}$ $\bar{5}$ 3
1	1.680	1.680	1 6 0
1	1.675	1.675	1 4 2
5	1.648	1.648	0 6 0

Diffraction data for crystal L3 were collected on the macromolecular beam line MX2 of the Australian Synchrotron using an ADSC Quantum 315r detector and monochromatic radiation with a wavelength of 0.7100 Å. A phi scan was employed with a framewidth of 1° and a counting time per frame of 1 s. The intensity data sets were processed using *XDS* software to produce data files which were analysed in *WinGX* (Farrugia, 1999). The refinements were made using *SHELXL-97* (Sheldrick, 2008). Further details of the data collection are reported in Table 3.

A structural model for the metal and oxygen atoms was obtained using *SHELXT* (Sheldrick, 2015) in space group $P\bar{1}$. It was found to be identical to that reported previously for crystals L1 and L2, corresponding to a laueite-type structure. The site occupancy for the divalent metal atom site *M*1 was fixed at the metal atom distribution obtained from the EMP analyses, 0.37Mn + 0.27Mg + 0.03Zn + 0.35Fe. The Fe/Al atomic ratios in sites *M*2 and *M*3 and the occupancy of the P site were refined. Difference-Fourier maps revealed the positions of nine H atoms. These were refined using soft restraints (Kampf *et al.*, 2014). The O–H distances were restrained to be 0.95(2) Å and the H–H distances for the water molecules were restrained to be 1.45(3) Å. An overall isotropic displacement parameter was employed for the H atoms. Refinement of anisotropic displacement parameters for all non-H atoms gave convergence at $R_1 = 0.032$ for all reflections to a resolution of 0.8 Å. Further details of the refinement are given in Table 3. The refined atomic coordinates, equivalent isotropic displacement parameters and site occupancies are reported in Table 4. Tables of anisotropic displacement parameters and observed and calculated structure factors have been deposited with the Principal Editor of *Mineralogical Magazine* and are available from http://www.minersoc.org/pages/e_journals/dep_mat_mm.html

The unit-cell composition from the structure refinement (refined site occupancies for *M*2, *M*3 and P, with OH adjusted for charge balance) is: $(Mn^{2+}_{0.37}Mg_{0.27}Zn_{0.03}Fe^{2+}_{0.33})_{\Sigma 1.00}(Fe^{3+}_{1.02}Al_{0.98})_{\Sigma 2.00}$

https://doi.org/10.1180/minmag.2016.080.061 Published online by Cambridge University Press

TABLE 3. Data collection and structure refinement details for kummerite.

Ideal formula	$MnFe^{3+}Al(PO_4)_2(OH)_2 \cdot 8H_2O$	
Formula weight	490.44	
Temperature	293(2) K	
Wavelength	0.7100 Å	
Crystal system	Triclinic	
Space group	$P\bar{1}$	
Unit-cell dimensions	$a = 5.3160(10)$ Å	$\alpha = 107.33(3)°$
	$b = 10.620(3)$ Å	$\beta = 111.33(3)°$
	$c = 7.1180(10)$ Å	$\gamma = 72.22(2)°$
Volume	348.45(16) $Å^3$	
Z	1	
Density (calculated)	2.337 g cm^{-3}	
Absorption coefficient	2.230 mm^{-1}	
F(000)	249	
Crystal size (mm)	0.04 × 0.02 × 0.005	
Theta range for data collection	4.102 to 26.343°	
Index ranges	$-6 <= h <= 6, -13 <= k <= 13, -8 <= l <= 8$	
Reflections collected	4231	
Independent reflections	1271 [R(int) = 0.0472]	
Completeness to theta = 25.214°	88.9%	
Refinement method	Full-matrix least-squares on F^2	
Data / restraints / parameters	1271 / 13 / 146	
Goodness-of-fit on F^2	1.103	
Final R indices [$I > 2\sigma(I)$]	$R_1 = 0.0317$, w$R_2 = 0.0863$	
R indices (all data)	$R_1 = 0.0325$, w$R_2 = 0.0870$	
Extinction coefficient	0.184(19)	
Largest diff. peak and hole	0.359 and –0.390 $e.Å^{-3}$	

$PO_4)_{1.95}(OH)_{2.15}(H_2O)_{7.85}$. This gives P_2O_5 28.0, Fe_2O_3 16.5 and Al_2O_3 10.1 wt.%, which agree with the (scaled) EMP analyses, P_2O_5 27.5, Fe_2O_3 17.4 and Al_2O_3 9.7 wt.% to within 1 standard deviation.

Crystal structure results

A projection of the structure of kummerite along [100] is shown in Fig. 6 with labelling of the anion sites and the dominant metals occupying the metal atom sites. The laueite-type sheets, parallel to {010}, are interconnected via corner-sharing between PO_4 tetrahedra and $MnO_2(H_2O)_4$ octahedra. The water molecules coordinated to Mn (in *trans*-pairs) are O7 and O8, while *trans*-pairs of water molecules coordinated to Al are labelled O6. A fourth water molecule, labeled O9, occupies the interlayer region.

The most important result from the structure refinement is the confirmation of ordering of dominant Fe in the octahedral site *M*2 and Al in the octahedral site *M*3. As shown in Table 4, the refined occupancies of these two sites give 59.3(8)% Fe in site *M*2 and 57.5(8)% Al in site *M*3. This is the basis of the acceptance of kummerite as a new mineral. It is the first laueite-group mineral to have ordering of different atoms in the *M*2 and *M*3 sites. The ordering is reflected in the shorter *M*3–O distances compared to the *M*2–O distances as shown in Table 5. The exception involves the *M*3–O6 distances, corresponding to coordinated water molecules. The site occupancies from the structure refinement were used in the calculation of bond valences, which are given in Table 6. These are consistent with site *M*1 containing only divalent elements and sites *M*2 and *M*3 containing trivalent elements.

All H atoms were located and their positions refined. These were used to establish the H-bonding, which is summarized in Table 7. The two strongest bonds, with O···O = 2.66 Å involve the water coordinated to Al, O6 as donor and a P-coordinated oxygen, O4, and the interlayer water molecule, O9, as acceptors. Medium strength bonds, with O···O distances of 2.74 to 2.81 Å, involve the hydroxyl anion, O5, and the water molecules, O7 to O9, as donors and the oxygen

https://doi.org/10.1180/minmag.2016.080.061 Published online by Cambridge University Press

TABLE 4. Refined coordinates ($\times 10^4$), site occupancy factors (s.o.f.) and equivalent isotropic displacement parameters ($Å^2 \times 10^3$) for kummerite.

Atom	s.o.f.	*x*	*y*	*z*	$U_{(eq)}$
Mn1	0.37	0	0	0	15(1)
Mg1	0.27	0	0	0	15(1)
Fe1	0.35	0	0	0	15(1)
Zn1	0.03	0	0	0	15(1)
Fe2	0.594(8)	0	5000	0	12(1)
Al2	0.406	0	5000	0	12(1)
Fe3	0.424(8)	0	5000	5000	13(1)
Al3	0.576	0	5000	5000	13(1)
P	0.973(5)	3445(1)	6688(1)	9256(1)	13(1)
O1		1663(4)	6530(2)	430(3)	17(1)
O2		2989(4)	5752(2)	7096(3)	17(1)
O3		2701(4)	8168(2)	9046(3)	18(1)
O4		3438(4)	3684(2)	9523(3)	16(1)
O5		1502(4)	5041(2)	2965(3)	17(1)
O6		2329(4)	3127(2)	5431(3)	19(1)
O7		2412(5)	69(2)	3207(4)	25(1)
O8		2268(4)	1099(2)	9442(4)	25(1)
O9		2679(4)	8026(2)	5079(3)	22(1)
H5*		3350(40)	4810(50)	3220(80)	46(4)
H6A		2900(90)	3270(50)	6820(30)	46(4)
H6B		3900(60)	2800(50)	5070(60)	46(4)
H7A		2490(100)	840(30)	4180(60)	46(4)
H7B		2090(100)	–500(40)	3760(60)	46(4)
H8A		1180(70)	1920(30)	9510(70)	46(4)
H8B		4010(40)	1170(40)	9860(70)	46(4)
H9A		2570(100)	8160(50)	6360(40)	46(4)
H9B		1770(90)	7380(40)	4270(60)	46(4)

*The numbering used for H atoms corresponds to the numbering of the coordinated oxygen.

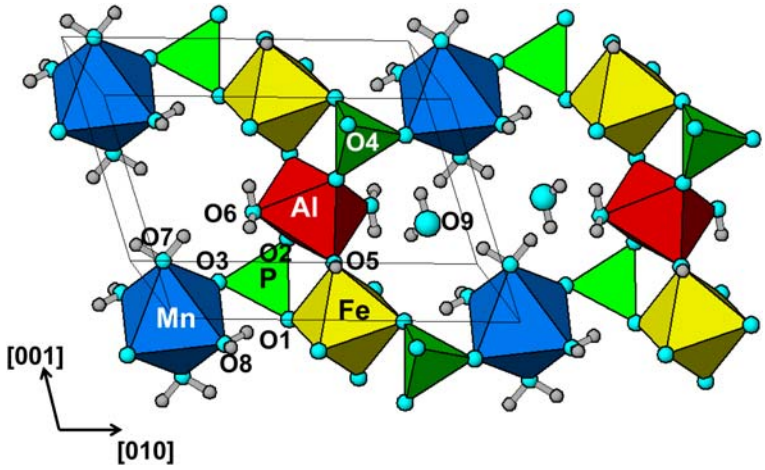

FIG. 6. Kummerite structure viewed along [100]. Small grey and blue spheres are hydrogen and oxygen.

https://doi.org/10.1180/minmag.2016.080.061 Published online by Cambridge University Press

TABLE 5. Polyhedral bond distances and water molecule geometries for kummerite.

*M*1–O8 (×2)	2.111(2)	O6–H6A	0.90(2)
–O3 (×2)	2.127(2)	–H6B	0.90(2)
–O7 (×2)	2.165(2)	H6A–O6–H6B	105(3)°
Average	2.134		
*M*2–O5 (×2)	1.958(2)	O7–H7A	0.90(2)
–O1 (×2)	1.975(2)	–H7B	0.89(2)
–O4 (×2)	2.004(2)	H7A–O7–H7B	105(3)°
Average	1.979		
*M*3–O5 (×2)	1.908(2)	O8–H8A	0.89(2)
–O2 (×2)	1.931(2)	–H8B	0.89(2)
–O6 (×2)	2.041(2)	H8A–O8–H8B	109(3)°
Average	1.960		
P–O3	1.539(2)	O9–H9A	0.90(2)
–O2	1.541(2)	–H9B	0.89(2)
–O1	1.543(2)	H9A–O9–H9B	107(3)°
–O4	1.554(2)		
Average	1.544		

atoms O1 to O3 of the PO_4 groups as acceptors. Almost identical H-bonding results, with O···O distances agreeing to better than 0.02 Å, have been reported from a single-crystal neutron diffraction study on the laueite-group mineral paravauxite by Gatta *et al.* (2014). These authors present diagrams of the H-bonding network, which are also applicable to kummerite.

TABLE 6. Bond valences for kummerite, calculated using the parameters of Brown and Altermatt (1985).

	M1*	M2*	M3*	P	H**	Σ
O1		$0.48^{\times2}\downarrow$		1.25	0.2	1.93
O2			$0.52^{\times2}\downarrow$	1.25	0.2	1.97
O3	$0.34^{\times2}\downarrow$			1.25	$0.2^{\times2}$	1.99
O4		$0.45^{\times2}\downarrow$		1.21	0.2	1.86
O5 (OH)		$0.50^{\times2}\downarrow$	$0.55^{\times2}\downarrow$		0.8	1.85
O6 (H_2O)			$0.40^{\times2}\downarrow$		$0.8^{\times2}$	2.00
O7 (H_2O)	$0.31^{\times2}\downarrow$				$0.8^{\times2}$	1.91
O8 (H_2O)	$0.36^{\times2}\downarrow$				$0.8^{\times2}$	1.96
Σ	2.02	2.86	2.94	4.96		

*$M1$ = 0.37Mn + 0.27Mg + 0.35Fe + 0.03Zn, $M2$ = 0.59Fe + 0.41Al; $M3$ = 0.42Fe + 0.58Al.
**From the H-bonding scheme given in Table 7.

Discussion

The structure of kummerite is shown in projection along [100] in Fig. 6. The key difference with respect to the laueite structure is the alternation of Fe^{3+} and Al^{3+} in the butlerite-type (Fanfani and Zanazzi, 1971) kinked chains of *trans*-connected octahedra running parallel to [001]. The two types of trivalent cations have different octahedral coordinations, $[FeO_4(OH)_2]^{7-}$ and $[AlO_2(OH)_2(H_2O)_2]^{3-}$, respectively, for sites *M*2 and *M*3. The Fe-centred octahedra share four vertices with PO_4 groups to form kröhnkite-type chains along [100], shown as horizontal chains in Fig. 1. The kröhnkite-type chains are interconnected along [001] by corner-sharing with the Al-centred octahedra. It is possible that the greater abundance

TABLE 7. Hydrogen bonds for kummerite.

D–H···A	*d*(D–H)	*d*(H···A)	*d*(D···A)	<(DHA) (°)
O5–H5···O2	0.90(2)	1.93(2)	2.802(3)	163(5)
O6–H6A···O4	0.903(19)	1.774(19)	2.668(3)	170(4)
O6–H6B···O9	0.900(19)	1.79(2)	2.669(3)	166(4)
O7–H7A···O6	0.902(19)	2.31(2)	3.155(3)	156(4)
O7–H7B···O9	0.893(19)	1.95(2)	2.811(3)	161(4)
O8–H8A···O1	0.889(19)	1.86(2)	2.739(3)	168(4)
O8–H8B···O3	0.887(19)	1.89(2)	2.756(3)	164(4)
O9–H9A···O3	0.904(19)	1.88(2)	2.778(3)	171(5)
O9–H9B···O5	0.891(19)	2.41(3)	3.223(3)	152(4)

https://doi.org/10.1180/minmag.2016.080.061 Published online by Cambridge University Press

TABLE 8. Comparative data for kummerite, laueite and mangangordonite.

	Kummerite	Laueite	Mangangordonite
Formula (ideal)	$Mn^{2+}Fe^{3+}Al(PO_4)_2(OH)_2\cdot 8H_2O$	$Mn^{2+}Fe_2^{3+}(PO_4)_2(OH)_2\cdot 8H_2O$	$Mn^{2+}Al_2^{3+}(PO_4)_2(OH)_2\cdot 8H_2O$
Symmetry	Triclinic, $P\bar{1}$	Triclinic, $P\bar{1}$	Triclinic, $P\bar{1}$
Cell	$a = 5.316(1)$ Å , $b = 10.620(3)$ Å $c = 7.118(1)$ Å, $\alpha = 107.33$ (3)°, $\beta = 111.33$ (3)°, $\gamma = 72.22$ (2)° $V = 348.4$ Å^3	$a = 5.28$ Å, $b = 10.66$ Å $c = 7.14$ Å, $\alpha = 107.9°$, $\beta = 110.9°$, $\gamma = 71.12°$ $V = 346.7$ Å^3	$a = 5.257$ Å, $b = 10.363$ Å $c = 7.040$ Å, $\alpha = 105.44°$, $\beta = 113.07°$, $\gamma = 78.69°$ $V = 333.3$ Å^3
Z	1	1	1
Strongest	9.885, 100 (010)	9.910, 100 (010)	4.77, 100 ($\bar{1}\bar{1}1$)
powder	4.942, 30 (020)	3.280, 90 (030)	6.39, 80 (001)
pattern lines	6.476, 20 (001)	4.950, 80 (011)	3.18, 70 (002)
d (Å), *I*, *hkl*	3.116, 18 ($1\bar{2}0$)	6.570, 70 (001)	9.96, 60 (010)
	2.873, 11 ($\bar{1}21$)	2.880, 60 (121)	2.86, 50 ($\bar{1}12$)
	3.988, 9 ($\bar{1}10$)	3.930, 50 (120)	2.59, 40 ($0\bar{3}2$)
Optics	Biaxial (–)	Biaxial (–)	Biaxial (+)
	$\alpha = 1.565(5)$, $\beta = 1.600(5)$, $\gamma = 1.630(5)$	$\alpha = 1.588$–1.603, $\beta = 1.654$–1.659, $\gamma = 1.680$–1.682	$\alpha = 1.556(1)$, $\beta = 1.561(2)$, $\gamma = 1.571(2)$
	2V(calc.) = 83.8°	2V(meas.) = 63–66°	2V(meas.) = 70°

of minerals having the laueite structure type relates to the presence of these strongly bonded kröhnkite chains. The other combinatorial polymorphs pseudolaueite, metavauxite and strunzite belong to a different topological graph (Krivovichev, 2004) in which the trivalent cations all have the same octahedral coordination, bonding to 3 $(PO4)^{3-}$, $2OH^-$ and 1 H_2O. Kröhnkite chains are not present in these minerals.

In the synthetic phases with ordered *M*2/*M*3 cations, the lower-valent, larger cation occupies the *M*3 site. In kummerite the situation is reversed and the smaller Al^{3+} cation occupies the *M*3 site. A possible explanation for this seemingly contradictory result is that kummerite has formed from laueite by Al^{3+} replacement for Fe^{3+} and that the replacement occurs preferentially at the site with the weaker bonds. In strunzite, $Mn^{2+}Fe_2^{3+}(PO_4)_2(OH)_2\cdot 6H_2O$ (Frondel, 1958), a topological isomer of the laueite structure type (Krivovichev, 2004), the two independent Fe^{3+} sites have the same octahedral coordination $FeO_3(OH)_2(H_2O)$.

TABLE 9. Laueite-supergroup minerals.

*M*1	*M*2	*M*3	Laueite group phosphates	Maghrebite group arsenates
Mn^{2+}	Fe^{3+}	Fe^{3+}	laueite[1]	
Mg^{2+}	Fe^{3+}	Fe^{3+}	ushkovite[2]	
Fe^{2+}	Fe^{3+}	Fe^{3+}	ferrolaueite[3]	césarferreiraite[8]
Mn^{2+}	Al^{3+}	Al^{3+}	mangangordonite[4]	
Mg^{2+}	Al^{3+}	Al^{3+}	gordonite[4]	maghrebite[9]
Fe^{2+}	Al^{3+}	Al^{3+}	paravauxite[5]	
Fe^{3+}	Al^{3+}	Al^{3+}	sigloite[6]	
Ba^{2+}	Al^{3+}	Al^{3+}	curetonite[7]	
Mn^{2+}	Fe^{3+}	Al^{3+}	kummerite	

References: [1]Moore (1965); [2]Galliski and Hawthorne (2002); [3]Segeler *et al.* (2012); [4]Leavens and Rheingold (1988); [5]Baur (1969); [6]Hawthorne (1988); [7]Cooper and Hawthorne (1994); [8]Scholz *et al.* (2014); [9]Meisser *et al.* (2012).

https://doi.org/10.1180/minmag.2016.080.061 Published online by Cambridge University Press

We have found that Al substitution in strunzite shows no preferential ordering, with the refinement of an Al-bearing strunzite giving 0.28(1)Al + 0.72(1)Fe in both Fe^{3+} sites (Grey *et al.*, 2012). It thus appears that the preferential ordering of Al in laueite is related to the different coordinations of the two Fe^{3+} sites. It follows that similar ordering of Al-substitution could be expected in stewartite, a laueite polymorph belonging to the same topological graph (Krivovichev, 2004).

Kummerite has a chemical composition halfway between that for laueite (Strunz, 1954; Moore, 1965) and for mangangordonite, $Mn^{2+}Al_2^{3+}(PO_4)_2(OH)_2{\cdot}8H_2O$ (Leavens and Rheingold, 1988), but with Al^{3+} and Fe^{3+} ordered. A comparison of properties for the three minerals is given in Table 8. Kummerite is the first laueite-group mineral with different cations ordered in the *M*2 and *M*3 sites. A representation of all minerals in the laueite supergroup is shown in Table 9.

Acknowledgements

The authors acknowledge access to the Macromolecular beam line MX2 at the Australian Synchrotron, for collection of the single-crystal X-ray data.

References

Adiwidjaja, G., Friese, K., Klaska, K.-H. and Schlüter, J. (1999) The crystal structure of kastningite (Mn,Fe,Mg)$(H_2O)_4[Al_2(OH)_2(H_2O)_2(PO_4)_2]{\cdot}2H_2O$ – a new hydroxyl aquated orthophosphate hydrate mineral. *Zeitschrift für Kristallographie*, **214**, 465–468.

Baur, W.H. (1969) The crystal structure of paravauxite, $FeAl_2(PO_4)_2(OH_2)_6(H_2O)_2$. *Neues Jahrbuch für Mineralogie Monatshafte*, **1969**, 430–433.

Birch, W.D., Grey, I.E., Mills, S.J., Pring, A. Wilson, N.C. and Keck, E. (2011) Nordgauite, $MnAl_2(PO_4)_2(F,OH)_2{\cdot}5.5H_2O$, a new mineral from the Hagendorf Süd pegmatite, Bavaria, Germany: description and crystal structure. *Mineralogical Magazine*, **75**, 269–278.

Brown, I.D. and Altermatt, D. (1985) Bond-valence parameters obtained from a systematic analysis of the inorganic crystal structure database. *Acta Crystallographica*, **B41**, 244–247.

Cavellec, M., Riou, D. and Ferey, G. (1994) Oxyfluorinated microporous compounds. XI. Synthesis and crystal structure of ULM-10: The first bidimensional mixed-valence iron fluorophosphates with intercalated ethylenediamine. *Journal of Solid State Chemistry*, **112**, 441–447.

Cooper, M. and Hawthorne, F.C. (1994) The crystal structure of curetonite, a complex heteropolyhedral sheet mineral. *American Mineralogist*, **79**, 545–549.

Fanfani, I. and Zanazzi, P.F. (1971) The crystal structure of butlerite. *American Mineralogist*, **56**, 751–757.

Farrugia, L.J. (1999) WinGX suite for small-molecule single-crystal crystallography. *Journal of Applied Crystallography*, **32**, 837–838.

Fleck, M., Kolitsch, U. and Hertweck, B. (2002) Natural and synthetic compounds with krohnkite-type chains: review and classification. *Zeitschrift für Kristallographie*, **217**, 435–443.

Frondel, C. (1958) Strunzite, a new mineral. *Naturwissenschaften*, **45**, 37.

Galliski, M.A. and Hawthorne, F.C. (2002) Refinement of the crystal structure of ushkovite from Nevados de Palermo, Republica Argentina. *The Canadian Mineralogist*, **40**, 929–937.

Gatta, G.D., Vignola, P. and Meven, M. (2014) On the complex H-bonding network in paravauxite, $Fe^{2+}Al_2(PO_4)_2(OH)_2{\cdot}8H_2O$: A single crystal neutron diffraction study. *Mineralogical Magazine*, **78**, 841–850.

Grey, I.E., Mumme, W.G., Neville, S.M., Wilson, N.C. and Birch, W.D. (2010) Jahnsite-whiteite solid solutions and associated minerals in the phosphate pegmatite at Hagendorf-Süd, Bavaria, Germany. *Mineralogical Magazine*, **74**, 969–978.

Grey, I.E., MacRae, C.M., Keck, E. and Birch, W.D. (2012) Aluminium-bearing strunzite derived from jahnsite at the Hagendorf-Süd pegmatite, Germany. *Mineralogical Magazine*, **76**, 1165–1174.

Grey, I.E., Keck, E., Mumme, W.G., Macrae, C.M., Price, J.R., Glenn, A.M. and Davidson, C.J. (2015) Crystallographic ordering of aluminium in laueite at Hagendorf-Süd. *Mineralogical Magazine*, **79**, 309–319.

Hawthorne, F.C. (1983) Graphical enumeration of polyhedral clusters. *Acta Crystallographica*, **A39**, 724–736.

Hawthorne, F.C. (1985) Towards a structural classification of minerals: The $^{VI}M^{IV}T_2\Phi_n$ minerals. *American Mineralogist*, **70**, 455–473.

Hawthorne, F.C. (1988) Sigloite: The oxidation mechanism in $[M_2^{3+}(PO_4)_2(OH)_2(H_2O)_2]^{2-}$ structures. *Mineralogy and Petrology*, **38**, 201–211.

Kampf, A.R., Hughes, J.M., Nash, B. and Marty, J. (2014) Kokinosite, $Na_2Ca_2(V_{10}O_{26}){\cdot}24H_2O$, a new decavanadate mineral species from the St. Jude mine, Colorado: crystal structure and descriptive mineralogy. *The Canadian Mineralogist*, **52**, 15–25.

Krivovichev, S.V. (2004) Topological and geometrical isomerism in minerals and inorganic compounds with laueite-type heteropolyhedral sheets. *Neues Jahrbuch für Mineralogie Monatshafte*, **2004**, 209–220.

Laugier, J. and Bochu, B. (2000) *LMGP-Program for the interpretation of X-ray experiments.* INPG/Laboratoire des Matériaux et du Génie Physique. St Martin d'Heres, France.

https://doi.org/10.1180/minmag.2016.080.061 Published online by Cambridge University Press

Leavens, P.B. and Rheingold, A.L. (1988) Crystal structures of gordonite, $MgAl_2(PO_4)_2(OH)_2(H_2O)_6(H_2O)_2$, and its Mn analog. *Neues Jahrbuch für Mineralogie Monatshafte*, **1988**, 265–270.

Libowitzky, E. (1999) Correlation of O–H stretching frequencies and O–H···O hydrogen bond lengths in minerals. Pp. 103–115 in: *Hydrogen Bond Research* (P. Schuster and W. Mikenda, editors). Springer-Verlag, Wien.

Locock, A.J. and Burns, P.C. (2003) The crystal structure of bergenite, a new geometrical isomer of the phosphuranylite group. *The Canadian Mineralogist*, **41**, 91–101.

Mandarino, J.A. (1981) The Gladstone-Dale relationship: Part IV. The compatibility concept and its application. *The Canadian Mineralogist*, **19**, 441–450.

Meisser, N., Brugger, J., Krivovichev, S., Armbruster, T. and Favreau, G. (2012) Description and crystal structure of maghrebite, $MgAl_2(ASO_4)_2(OH)_2{\cdot}8H_2O$, from Aghbar, Anti-Atlas, Morocco: first arsenate in the laueite mineral group. *European Journal of Mineralogy*, **24**, 717–726.

Mills, S.J. and Grey, I.E. (2015) Nomenclature for the laueite supergroup. *Mineralogical Magazine*, **79**, 243–246.

Moore, P.B. (1965) The crystal structure of laueite, $Mn^{2+}Fe_2^{3+}(OH)_2(PO_4)_2(H_2O)_6{\cdot}2H_2O$. *American Mineralogist*, **50**, 1884–1892.

Moore, P.B. (1975) Laueite, pseudolaueite, stewartite and metavauxite: A study in combinatorial polymorphism. *Neues Jahrbuch für Mineralogie Abhandlugen*, **1975**, 148–159.

Moore, P.B. and Araki, T. (1974) Stewartite, $Mn^{2+}Fe_2^{3+}(OH)_2(H_2O)_6[PO_4]_3{\cdot}2H_2O$: Its atomic arrangement. *American Mineralogist*, **59**, 1272–1276.

Scholz, R., Chukanov, N.V., Menezes Filho, L.A.D., Attencio, D., Lagoeiro, L., Belotti, F.M., Chaves, M.L. S.C., Romano, A.W., Brandao, P.R., Belakovskiy, D.I. and Pekov, I. (2014) Césarferreiraite, $Fe^{2+}Fe_2^{3+}(AsO_4)_2(OH)_2{\cdot}8H_2O$, from Eduardo mine, Conselheiro Pena, Minas Gerais, Brazil: Second arsenate in the laueite mineral group. *American Mineralogist*, **99**, 607–611.

Segeler, C.G., Moore, P.B., Dyar, M.D., Leans, F. and Ferraiolo, J.A. (2012) Ferrolaueite, a new mineral from Monmouth County, New Jersey, USA. *Australian Journal of Mineralogy*, **16**, 69–76.

Sheldrick, G.M. (2008) A short history of SHELX. *Acta Crystallographica*, **A64**, 112–122.

Sheldrick, G.M. (2015) SHELXT-Integrated space-group and crystal-structure determination. *Acta Crystallographica*, **A71**, 3–8.

Strunz, H. (1954) Laueit, $MnFe_2^{III}(PO_4)_2(OH)_2{\cdot}8H_2O$, ein neues Mineral. *Naturwissenschaften*, **41**, 256.

Wang, X., Liu, L., Cheng, H., Ross, K. and Jacobson, A.J. (2000) Synthesis and crystal structures of $[H_3N(CH_2)_2NH_3]NbMOF(PO_4)_2(H_2O)_2$, M = Fe, Co and $[H_3N(CH_2)_2NH_3]Ti(Fe_{0.9}Cr_{0.1})F_{1.3}O_{0.7})(H_{0.3}PO_4)_2(H_2O)_2$. *Journal of Materials Chemistry*, **10**, 1203–1208.

https://doi.org/10.1180/minmag.2016.080.061 Published online by Cambridge University Press